2007-11-01

Polarization Rotation Correction in Radiometry: An Error Analysis

David G. Long
david_long@byu.edu

Derek Hudson

Jeffrey R. Piepmeier

Original Publication Citation

Hudson, D., J. R. Piepmeier, and D. G. Long. "Polarization Rotation Correction in Radiometry: An Error Analysis." Geoscience and Remote Sensing, IEEE Transactions on 45.1 (27): 3212-23

Polarization Rotation Correction in Radiometry: An Error Analysis

Derek Hudson, Jeffrey R. Piepmeier, *Member, IEEE*, and David G. Long, *Senior Member, IEEE*

***Abstract*—Yueh proposed a method of using the third Stokes parameter T_U to correct brightness temperatures such as T_v and T_h for polarization rotation. This paper presents an extended error analysis of the estimation of T_v, T_h, and $T_Q \equiv T_v - T_h$ by Yueh's method. In order to carry out the analysis, we first develop a forward model of polarization rotation that accounts for the random nature of thermal radiation, receiver noise, and (to first order) calibration. Analytic formulas are then derived for the bias, standard deviation (STD), and root-mean-square error (RMSE) of estimated T_Q, T_v, and T_h, as functions of scene and radiometer parameters. These formulas are validated through independent calculation via Monte Carlo simulation. Examination of the formulas reveals that: 1) natural T_U from planetary surface radiation, of the magnitude expected on Earth at L-band, has a negligible effect on correction for polarization rotation; 2) RMSE is a function of rotation angle Ω, but the value of Ω that minimizes RMSE is not known prior to instrument fabrication; and 3) if residual calibration errors can be sufficiently reduced via postlaunch calibration, then Yueh's method reduces the error incurred by polarization rotation to negligibility.**

***Index Terms*—Faraday effect, microwave polarimetry, polarization.**

I. Introduction

THE EARTH'S ionosphere and magnetic field cause Faraday rotation of the polarization of radiation emanating from the Earth's surface. This rotation mixes the vertical and horizontal polarization components of brightness temperatures T_v and T_h, degrading the measurement of both. The oft-used second Stokes parameter T_Q ($\equiv T_v - T_h$) is doubly degraded. For L-band satellite measurements, the error in T_Q due to uncorrected Faraday rotation can exceed 10 K, depending on solar activity, incidence angle, and the angle between the look direction and the Earth's magnetic field [2] (Faraday rotation is inversely proportional to the square of frequency; therefore, this source of polarization rotation is less important above L-band).

Additional polarization rotation occurs if a sensor's antenna feed polarization basis is rotated with respect to the natural polarization basis of the Earth's surface. Such rotation may occur as an accidental misalignment [3] or may be deliberately permitted in order to simplify hardware [4].

Near-future L-band spaceborne radiometers, namely, SMOS [5] and Aquarius [6], are being designed to perform polarization rotation correction (PRC) in postprocessing. A basic method involves measuring the third Stokes parameter T_U in addition to the usual T_v and T_h. The method is introduced by Yueh in [1].

Previously developed forward models of polarization rotation [1], [3], [4], [7] are deterministic and neglect the role of receiver channel noise (although [8] includes noise in simulations). In the Appendix, we develop an extended model which takes into account the random nature of the radiation and also accounts for receiver noise. Simple and accurate expressions are derived for the means, variances, and covariances of the measurements in a three-channel (T_v, T_h, and T_U) radiometer. These are derived in the Appendix and summarized in Section II.

In Section III, we review Yueh's correction technique. In Section IV, we derive the mean, variance, and root-mean-square error (RMSE) of the resulting estimate of T_Q. Similar derivations for T_v and T_h are presented in Section V. Insights from the resulting formulas are presented in Section VI, and conclusions are offered in Section VII.

Throughout this paper, we illustrate with case studies of the Aquarius radiometer, whose deployment is expected in 2009. The Aquarius instrument will have three beams with respective incidence angles of 28.7°, 37.8°, and 45.6° [6]. For measurements of ocean emissions, these angles dictate a nominal T_Q of about 20, 35, and 53 K, respectively [9]. The Aquarius instrument also has nominal integration time τ of 6 s. We also refer to the canceled NASA Hydros mission [10], whose nominal τ was 0.016 s (we adjust the Hydros incidence angle from 39.3° to 37.8° in our studies to match Aquarius).

II. Summary of Forward Model

As shown in the Appendix, the processes of receiving, detecting, and calibrating the first three Stokes parameters in a polarimetric radiometer can be summarized with the forward model

$$\hat{T}_{Ia} = T_I + \Delta T_{\mathrm{RX},I} + \Delta T_{\mathrm{sys},I} \quad (1)$$

$$\hat{T}_{Qa} = +T_Q \cos 2\Omega + T_U \sin 2\Omega + \Delta T_{\mathrm{RX},Q} + \Delta T_{\mathrm{sys},Q} \quad (2)$$

$$\hat{T}_{Ua} = -T_Q \sin 2\Omega + T_U \cos 2\Omega + \Delta T_{\mathrm{RX},U} + \Delta T_{\mathrm{sys},U}. \quad (3)$$

Manuscript received September 29, 2006; revised March 27, 2007. This work was supported by the NASA Goddard Space Flight Center.

D. Hudson and D. G. Long are with the Department of Electrical and Computer Engineering, Brigham Young University, Provo, UT 84602 USA (e-mail: dlh8@et.byu.edu).

J. R. Piepmeier is with the Microwave Instrument Technology Branch, NASA Goddard Space Flight Center, Greenbelt, MD 20771 USA.

Color versions of one or more of the figures in this paper are available online at http://ieeexplore.ieee.org.

Digital Object Identifier 10.1109/TGRS.2007.898438

The quantities on the left-hand sides are our measurements of the first three Stokes parameters after rotation, detection, and calibration. On the right sides, the natural Stokes parameters of the scene T_I, T_Q, and T_U are altered by polarization rotation Ω [7] and perturbed by error sources, represented by quantities with a Δ prefix.

$\Delta T_{\mathrm{RX},I}$, $\Delta T_{\mathrm{RX},Q}$, and $\Delta T_{\mathrm{RX},U}$ are residual biases from the calibration process that is performed throughout data collection. For example, if the fourth calibration scheme described in [11] is used, then $\Delta T_{\mathrm{RX},U}$ corresponds to all but the first term on the right side of [11, eq. (42)]. That same calibration scheme also leads to

$$\Delta T_{\mathrm{RX},v} = \Delta T_{\mathrm{RX},h} = \frac{T_{\mathrm{H}}\hat{T}_{\mathrm{C}} - T_{\mathrm{C}}\hat{T}_{\mathrm{H}}}{T_{\mathrm{H}} - T_{\mathrm{C}}} \tag{4}$$

where T_{H} and T_{C} are the true temperatures of the hot and cold calibration sources, while $\hat{T}_{\mathrm{H}}$ and $\hat{T}_{\mathrm{C}}$ are the best available estimates of them (the calibration sources could be noise diodes or external targets, for example). Then, $\Delta T_{\mathrm{RX},I}$ and $\Delta T_{\mathrm{RX},Q}$ are defined as the sum and difference of $\Delta T_{\mathrm{RX},v}$ and $\Delta T_{\mathrm{RX},h}$, respectively.

Using (4) gives $\Delta T_{\mathrm{RX},Q} = 0$. A more realistic description distinguishes between the calibration sources in the v and h channels, i.e.,

$$\begin{aligned}\Delta T_{\mathrm{RX},v} &= \frac{T_{\mathrm{H}v}\hat{T}_{\mathrm{C}v} - T_{\mathrm{C}v}\hat{T}_{\mathrm{H}v}}{T_{\mathrm{H}v} - T_{\mathrm{C}v}} \\ \Delta T_{\mathrm{RX},h} &= \frac{T_{\mathrm{H}h}\hat{T}_{\mathrm{C}h} - T_{\mathrm{C}h}\hat{T}_{\mathrm{H}h}}{T_{\mathrm{H}h} - T_{\mathrm{C}h}}\end{aligned} \tag{5}$$

so that $\Delta T_{\mathrm{RX},Q}$ is nonzero. This distinction also complicates the expression for $\Delta T_{\mathrm{RX},U}$.

The radiometer calibration process is such that $\Delta T_{\mathrm{RX},I}$, $\Delta T_{\mathrm{RX},Q}$, and $\Delta T_{\mathrm{RX},U}$ are slowly varying (e.g., over a period of many minutes or more) compared with the radiometer integration time τ. Even if estimates of the calibration parameters (e.g., $\hat{T}_{Cv}$) are obtained as often as several times per τ, we assume that the predictable thermal environment of space allows us to average those estimates extensively to yield better estimates. Therefore, for estimating T_v, T_h, and T_Q measured in a single radiometer measurement cycle or even many cycles, we can consider $\Delta T_{\mathrm{RX},I}$, $\Delta T_{\mathrm{RX},Q}$, and $\Delta T_{\mathrm{RX},U}$ to be constants. It is also anticipated that this averaging (and other postlaunch calibration activities) will reduce $\Delta T_{\mathrm{RX},I}$, $\Delta T_{\mathrm{RX},Q}$, and $\Delta T_{\mathrm{RX},U}$ to such low magnitude that they are negligible compared to the other error sources.

In the development of (1)–(3), we have neglected the channel gains which are also estimated during data collection as part of the calibration process (see [11]). Although these gains and our uncertainties in them are relevant, we omit them in this paper, leaving their analysis for future work.

The quantities $\Delta T_{\mathrm{sys},I}$, $\Delta T_{\mathrm{sys},Q}$, and $\Delta T_{\mathrm{sys},U}$ in (1)–(3) are zero-mean Gaussian random variables which correspond to the usual noise equivalent ΔT $(\mathrm{NE}\Delta T)$ of radiometric measurements [12, p. 365]. They fluctuate significantly from one radiometer measurement cycle to the next. From their definition in (67)–(69), we see that they have the same covariance matrix as $\hat{T}_{\mathrm{sys},I}$, $\hat{T}_{\mathrm{sys},Q}$, and $\hat{T}_{\mathrm{sys},U}$ (as well as $\hat{T}_{Ia}$, $\hat{T}_{Qa}$, and $\hat{T}_{Ua}$), which is given in (66). In (66), $N \equiv 2B\tau$, where B is the sensor bandwidth (about 20 MHz for Aquarius and Hydros).

For future reference, we find the means of our calibrated measurements:

$$\begin{aligned}T_{Ia} &\equiv \langle \hat{T}_{Ia} \rangle = T_I + \Delta T_{\mathrm{RX},I} \\ T_{Qa} &\equiv \langle \hat{T}_{Qa} \rangle = +T_Q \cos 2\Omega + T_U \sin 2\Omega + \Delta T_{\mathrm{RX},Q} \\ T_{Ua} &\equiv \langle \hat{T}_{Ua} \rangle = -T_Q \sin 2\Omega + T_U \cos 2\Omega + \Delta T_{\mathrm{RX},U}.\end{aligned} \tag{6}$$

III. Rotation Correction Technique

In this section, we review PRC in the context of the forward model summarized in Section II.

A. Estimation of T_Q

Yueh's model [1] does not include any of the Δ terms in (1)–(3). By noting that T_U is much smaller than T_Q in natural Earth scenes, he proposes to solve (2) and (3) for T_Q by also neglecting the terms with T_U. By assuming T_U and all the Δ quantities are zero, squaring both sides of (2) and (3), adding the two results, and then solving for T_Q, we obtain Yueh's proposed estimate

$$\hat{T}_Q = \sqrt{\hat{T}_{Qa}^2 + \hat{T}_{Ua}^2} \tag{7}$$

where we ignore the negative root since T_Q is positive in geophysical circumstances. In reality, of course, T_U and all the Δ quantities are nonzero and constitute the error sources of the correction technique. Nevertheless, as demonstrated by the error analysis in Section IV, this equation provides a good estimate of T_Q.

B. Estimation of T_v and T_h

With $\hat{T}_Q$ from (7) and $\hat{T}_{Ia}$ from (1), we can also find $\hat{T}_v$ and $\hat{T}_h$ as $(\hat{T}_{Ia} \pm \hat{T}_Q)/2$. An error analysis of $\hat{T}_v$ and $\hat{T}_h$ is pursued in Section V.

Yueh proposed an alternate method of estimating $\hat{T}_v$ and $\hat{T}_h$ (although it is straightforward to show its equivalence to estimating $\hat{T}_v$ and $\hat{T}_h$ via $(\hat{T}_{Ia} \pm \hat{T}_Q)/2$). First, to estimate Ω, we divide (3) by (2), then solve for Ω. With the error sources (T_U and all the Δ quantities) assumed to be zero, this yields

$$\hat{\Omega} = \frac{1}{2}\tan^{-1}\frac{-\hat{T}_{Ua}}{\hat{T}_{Qa}} \tag{8}$$

as an estimate of the angle of polarization rotation. Then, assuming the error sources are zero and solving (73) and (74) for T_v and T_h, respectively, yields

$$\hat{T}_v = \hat{T}_{va} + \hat{T}_Q \sin^2 \hat{\Omega} \tag{9}$$

$$\hat{T}_h = \hat{T}_{ha} - \hat{T}_Q \sin^2 \hat{\Omega} \tag{10}$$

which are the corrected forms of [1, eqs. (15) and (16)], where $\hat{T}_Q$ is given in (7).

IV. Analysis of $\hat{T}_Q$

We now determine the probability density function (pdf), mean, and variance of the estimate $\hat{T}_Q = \sqrt{\hat{T}_{Qa}^2 + \hat{T}_{Ua}^2}$. We use the mean and variance to calculate RMSE. $\hat{T}_{Qa}$ and $\hat{T}_{Ua}$ are already well characterized. They are Gaussian (at least to a very good approximation) with means given in (6) and with variances and covariance given in (66).

A. Rotation of Variables

$\hat{T}_{Qa}$ and $\hat{T}_{Ua}$ are correlated, but we can rotate coordinates such that we have uncorrelated quantities. Define

$$\begin{bmatrix} \hat{Z} \\ \hat{W} \end{bmatrix} = \frac{1}{\sqrt{T_{\mathrm{sys},Q}^2 + T_{\mathrm{sys},U}^2}} \begin{bmatrix} T_{\mathrm{sys},Q} & T_{\mathrm{sys},U} \\ -T_{\mathrm{sys},U} & T_{\mathrm{sys},Q} \end{bmatrix} \begin{bmatrix} \hat{T}_{Qa} \\ \hat{T}_{Ua} \end{bmatrix}. \quad (11)$$

This is useful because $\sqrt{\hat{Z}^2 + \hat{W}^2} = \sqrt{\hat{T}_{Qa}^2 + \hat{T}_{Ua}^2} = \hat{T}_Q$. If we assume that $\hat{T}_{Qa}$ and $\hat{T}_{Ua}$ are *jointly* normal, then $\hat{Z}$ and $\hat{W}$ are also jointly normal, and it is straightforward to show that $\hat{Z}$ and $\hat{W}$ are uncorrelated and have the following means and variances:

$$\langle \hat{Z} \rangle = \frac{T_{\mathrm{sys},Q} T_{Qa} + T_{\mathrm{sys},U} T_{Ua}}{\sqrt{T_{\mathrm{sys},Q}^2 + T_{\mathrm{sys},U}^2}} \equiv Z \quad (12)$$

$$\langle \hat{W} \rangle = \frac{T_{\mathrm{sys},Q} T_{Ua} - T_{\mathrm{sys},U} T_{Qa}}{\sqrt{T_{\mathrm{sys},Q}^2 + T_{\mathrm{sys},U}^2}} \equiv W \quad (13)$$

$$\mathrm{Var}(\hat{Z}) = \frac{T_{\mathrm{sys},I}^2 + T_{\mathrm{sys},Q}^2 + T_{\mathrm{sys},U}^2}{N} \equiv \sigma_Z^2 \quad (14)$$

$$\mathrm{Var}(\hat{W}) = \frac{T_{\mathrm{sys},I}^2 - T_{\mathrm{sys},Q}^2 - T_{\mathrm{sys},U}^2}{N} \equiv \sigma_W^2. \quad (15)$$

The pdf of $\hat{T}_Q$ is given by using Z, W, σ_Z, and σ_W in [13, eq. (2)], which is restated here in terms of the current problem:

$$f_{\hat{T}_Q}(\hat{T}_Q) = \frac{\hat{T}_Q}{\sigma_Z \sigma_W} e^{-\frac{\hat{T}_Q^2 + 2Z^2}{4\sigma_Z^2}} e^{-\frac{\hat{T}_Q^2 + 2W^2}{4\sigma_W^2}} \cdot \sum_{j=-\infty}^{\infty} I_j\left(a\hat{T}_Q^2\right) I_{2j}(d\hat{T}_Q) \cos 2j\psi \quad (16)$$

for $\hat{T}_Q > 0$ and 0 otherwise, where

$$a \equiv \frac{\sigma_Z^2 - \sigma_W^2}{4\sigma_Z^2 \sigma_W^2}$$

$$d^2 \equiv \frac{Z^2}{\sigma_Z^4} + \frac{W^2}{\sigma_W^4}$$

$$\tan\psi \equiv \frac{W\sigma_Z^2}{Z\sigma_W^2}$$

and I_j is the modified Bessel function of the first kind and order j.

B. Simple Result by Assuming $\sigma_Z^2 \approx \sigma_W^2$

We attempted to find the first and second moments of $\sqrt{\hat{Z}^2 + \hat{W}^2}$ analytically but failed, even though the pdf is known. Fortunately, a small approximation leads to simple and accurate formulas, as shown now.

$T_{\mathrm{sys},Q}^2 + T_{\mathrm{sys},U}^2$ has a worst case maximum value of about 4000 K^2 for Aquarius; in more extreme cases, it might reach 10 000 K^2 (this is for L-band radiometers with incidence angles less than about 50°). But, this is small compared to $T_{\mathrm{sys},I}^2$, which has a value of 660 000 K^2 for typical Aquarius parameters ($T_{\mathrm{RX},I} = 620$ K and $T_I = 190$ K). Therefore, $\sigma_Z^2 \approx T_{\mathrm{sys},I}^2/N$ and $\sigma_W^2 \approx T_{\mathrm{sys},I}^2/N$.

If we define $\sigma^2 \equiv T_{\mathrm{sys},I}^2/N$ and use $\sigma_Z^2 \approx \sigma^2$ and $\sigma_W^2 \approx \sigma^2$, then $\hat{T}_Q$ is the root of the sum of the squares of two independent Gaussians with the same variance and with nonzero, unequal means. Note that σ is the $\mathrm{NE}\Delta T$ for the total signal (first Stokes parameter).

With this approximation, the pdf, mean, and variance of $\hat{T}_Q$ can be described as functions of just σ and m, where $m^2 \equiv Z^2 + W^2 = T_{Qa}^2 + T_{Ua}^2$. In terms of the original parameters

$$\begin{aligned} m^2 = {} & T_Q^2 + T_U^2 + \Delta T_{\mathrm{RX},Q}^2 + \Delta T_{\mathrm{RX},U}^2 \\ & + 2\cos 2\Omega(+T_Q \Delta T_{\mathrm{RX},Q} + T_U \Delta T_{\mathrm{RX},U}) \\ & + 2\sin 2\Omega(-T_Q \Delta T_{\mathrm{RX},U} + T_U \Delta T_{\mathrm{RX},Q}). \end{aligned} \quad (17)$$

By either [14] or by [13, eq. (1)], the density of $\hat{T}_Q$ is then

$$f_{\hat{T}_Q}(\hat{T}_Q) = \frac{\hat{T}_Q}{\sigma^2} e^{-\frac{\hat{T}_Q^2 + m^2}{2\sigma^2}} I_0\left(\frac{\hat{T}_Q m}{\sigma^2}\right), \quad \hat{T}_Q > 0 \text{ (0 otherwise)}. \quad (18)$$

The mean and variance of $\hat{T}_Q$ are [15, p. 72]

$$\langle \hat{T}_Q \rangle = \sigma\sqrt{\frac{\pi}{2}} e^{-\frac{m^2}{2\sigma^2}} {}_1F_1\left(\frac{3}{2}, 1; \frac{m^2}{2\sigma^2}\right) \quad (19)$$

$$\mathrm{Var}(\hat{T}_Q) = 2\sigma^2 + m^2 - \langle \hat{T}_Q \rangle^2 \quad (20)$$

where ${}_1F_1$ is the confluent hypergeometric function.

Equation (19) corresponds with the first line of (3.10–12) in [16]; the second line shows that we can rewrite $\langle \hat{T}_Q \rangle$ as

$$\langle \hat{T}_Q \rangle = \sigma\sqrt{\frac{\pi}{2}} {}_1F_1\left(-\frac{1}{2}, 1; -\frac{m^2}{2\sigma^2}\right). \quad (21)$$

A difficulty with using either (19) or (21) is that for large τ, σ is small, and the argument of ${}_1F_1$ has very large magnitude (e.g., 70 000 for the Aquarius $\theta = 28.7°$ case). Calculating the value of ${}_1F_1$ to high precision presents a huge computational burden when its argument is so large.

Fortunately, using (4B-9) in [16], (21) becomes

$$\langle \hat{T}_Q \rangle = \sigma \sqrt{\frac{\pi}{2}} e^{-\frac{m^2}{4\sigma^2}} \left[\left(1 + \frac{m^2}{2\sigma^2} \right) I_0 \left(\frac{m^2}{4\sigma^2} \right) + \frac{m^2}{2\sigma^2} I_1 \left(\frac{m^2}{4\sigma^2} \right) \right] \tag{22}$$

which can be evaluated quickly.

The final simplification comes by examining plots of Monte Carlo results (see Section IV-C2). These plots suggest that $\mathrm{Var}(\hat{T}_Q) \approx \sigma^2$. Hypothesizing that $\mathrm{Var}(\hat{T}_Q) \approx \sigma^2$ is correct and using this in (20) yields the simple formulas

$$\langle \hat{T}_Q \rangle \approx \sqrt{\sigma^2 + m^2} \tag{23}$$

$$\Rightarrow \mathrm{Bias}(\hat{T}_Q) \approx \sqrt{\sigma^2 + m^2} - T_Q \tag{24}$$

$$\mathrm{Var}(\hat{T}_Q) \approx \sigma^2 \text{ (our hypothesis)} \tag{25}$$

$$\Rightarrow \text{RMSE of } \hat{T}_Q = \sqrt{\mathrm{Var}(\hat{T}_Q) + \mathrm{Bias}^2(\hat{T}_Q)} \approx \sqrt{2\sigma^2 + m^2 + T_Q^2 - 2T_Q\sqrt{\sigma^2 + m^2}}. \tag{26}$$

These equations are the key results of this paper.

We note that the pdf of $\hat{T}_Q$ given in (18) can be well approximated by a Gaussian pdf with the mean and variance of (23) and (25). Therefore, we are justified in ignoring higher moments hereafter and concerning ourselves with only the mean and variance (and the RMSE derived from them).

C. Validation of (23)–(26)

In this section, we use numerical methods to validate the derivation of (23)–(26).

1) Numerical Equivalence of (22) and (23): We can validate the final leap used to obtain (23) by showing that (23) matches (22). A mathematics software package finds the magnitude of the difference between (22) and (23) to be less than 20 nK in the Aquarius $\theta = 28.7^\circ$ case and less than 60 nK in the other Aquarius cases (these are calculated with $T_U = \Delta T_{\mathrm{RX},Q} = 0.5$ K, $\Delta T_{\mathrm{RX},U} = 0$ K, and typical Aquarius values of T_Q, T_I, $T_{\mathrm{RX},I}$, and N for $-180^\circ \le \Omega \le 180^\circ$).

2) Validation by Monte Carlo Simulation of Electric-Field Model: The mean and variance of $\hat{T}_Q$ can also be found by Monte Carlo simulation. This can be done using (39) and (48) directly, thus avoiding all the approximations used in deriving (23)–(26) from (39) and (48).

The precise procedure is to generate N samples of a, b, E_v, and E_h, which are all independent of one another except $\langle E_v E_h \rangle = T_U/2$. From these, N samples of x and y are formed according to (39) and then squared and averaged to produce a single sample each of $\hat{T}_{\mathrm{sys},Q}$ and $\hat{T}_{\mathrm{sys},U}$ as in (48). To simulate the calibration process, $T_{\mathrm{RX},Q}$ is subtracted off, while $\Delta T_{\mathrm{RX},Q}$ and $\Delta T_{\mathrm{RX},U}$ are added on, forming $\hat{T}_{Qa}$ and $\hat{T}_{Ua}$ as in (2) and (3). These are used in (7) to form a single sample of $\hat{T}_Q$. This entire procedure is repeated M times to form M independent samples of $\hat{T}_Q$. The empirical mean and variance of $\hat{T}_Q$ can then be calculated from these samples. This method gives no formulas, but its results converge to the exact results as M increases.

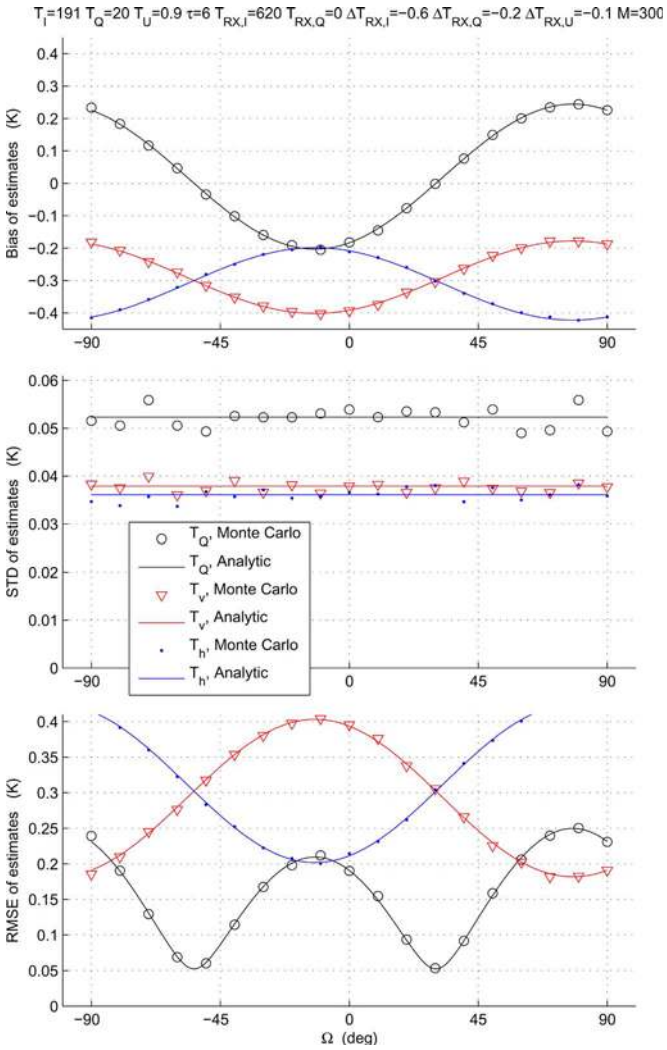

Fig. 1. (Top) Bias, (center) STD, and (bottom) RMSE of $\hat{T}_Q$, $\hat{T}_v$, and $\hat{T}_h$ as functions of Ω, with T_I, T_Q, τ, and $T_{\mathrm{RX},I}$ chosen to be typical of the Aquarius $\theta = 28.7^\circ$ beam over ocean. The values of the remaining parameters ($T_{\mathrm{RX},Q}$, $\Delta T_{\mathrm{RX},I}$, $\Delta T_{\mathrm{RX},Q}$, and $\Delta T_{\mathrm{RX},U}$) were chosen arbitrarily within expected ranges.

The Monte Carlo results match the analytic results from (24)–(26) very well, for many values of each of the parameters. Figs. 1–4 show some of these results. The discrepancy can be attributed to the inherent imprecision in the Monte Carlo method.

V. Analysis of $\hat{T}_v$ and $\hat{T}_h$

We now pursue an analysis of $\hat{T}_v$ and $\hat{T}_h$, which are defined as $(\hat{T}_{Ia} \pm \hat{T}_Q)/2$. Using (1) and (23)

$$\langle \hat{T}_v \rangle \approx \frac{1}{2} \left[T_I + \Delta T_{\mathrm{RX},I} + \sqrt{\sigma^2 + m^2} \right] \tag{27}$$

$$\langle \hat{T}_h \rangle \approx \frac{1}{2} \left[T_I + \Delta T_{\mathrm{RX},I} - \sqrt{\sigma^2 + m^2} \right]. \tag{28}$$

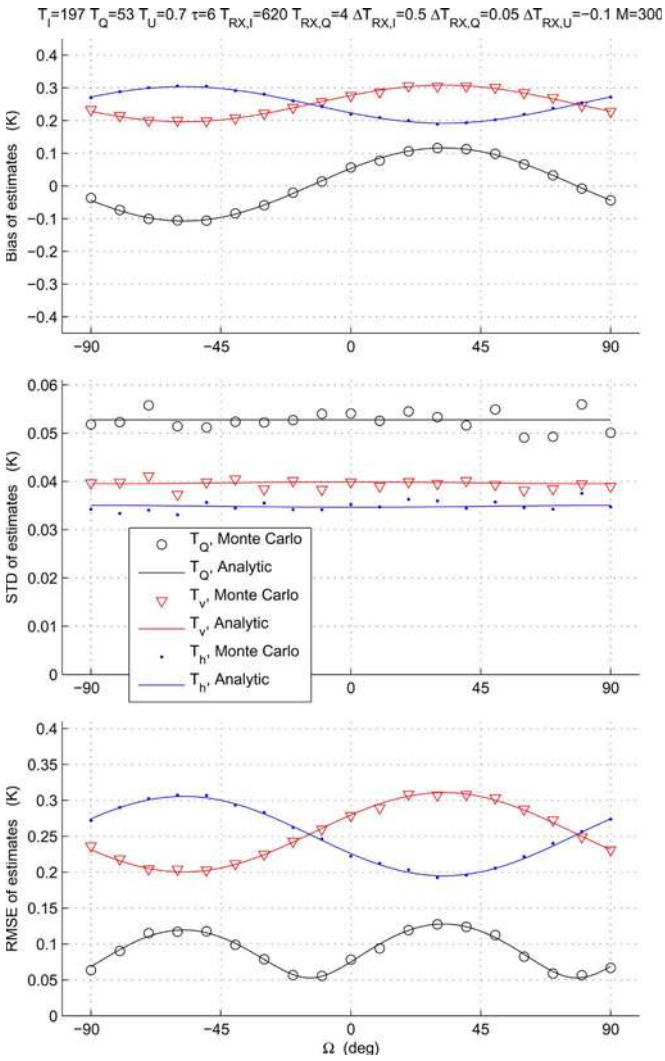

Fig. 2. Same as Fig. 1 except for the Aquarius $\theta = 45.6^\circ$ beam (different choices of $T_{\mathrm{RX},Q}$, $\Delta T_{\mathrm{RX},I}$, $\Delta T_{\mathrm{RX},Q}$, and $\Delta T_{\mathrm{RX},U}$ were also used in order to demonstrate the variety of possible behavior in the error).

A. *Variance and RMSE of $\hat{T}_v$ and $\hat{T}_h$*

Using (66) and (25)

$$\begin{aligned}\mathrm{Var}(\hat{T}_v) &= \frac{1}{4}\left[\mathrm{Var}(\hat{T}_{Ia})+\mathrm{Var}(\hat{T}_Q)+2\mathrm{Cov}(\hat{T}_{Ia},\hat{T}_Q)\right] \\ &\approx \frac{1}{4}\left[\frac{2T_{\mathrm{sys},I}^2+T_{\mathrm{sys},Q}^2+T_{\mathrm{sys},U}^2}{N}+2\mathrm{Cov}(\hat{T}_{Ia},\hat{T}_Q)\right].\end{aligned} \tag{29}$$

Similarly

$$\mathrm{Var}(\hat{T}_h) \approx \frac{1}{4}\left[\frac{2T_{\mathrm{sys},I}^2+T_{\mathrm{sys},Q}^2+T_{\mathrm{sys},U}^2}{N}-2\mathrm{Cov}(\hat{T}_{Ia},\hat{T}_Q)\right]. \tag{30}$$

Finding $\mathrm{Cov}(\hat{T}_{Ia},\hat{T}_Q)$ analytically appears to be intractable. But, from (29) and (30), we see that $\mathrm{Cov}(\hat{T}_{Ia},\hat{T}_Q) = \mathrm{Var}(\hat{T}_v) - \mathrm{Var}(\hat{T}_h)$. We can therefore find $\mathrm{Cov}(\hat{T}_{Ia},\hat{T}_Q)$ numerically by subtracting the Monte Carlo estimates of $\mathrm{Var}(\hat{T}_h)$ from the Monte Carlo estimates of $\mathrm{Var}(\hat{T}_v)$. We studied such

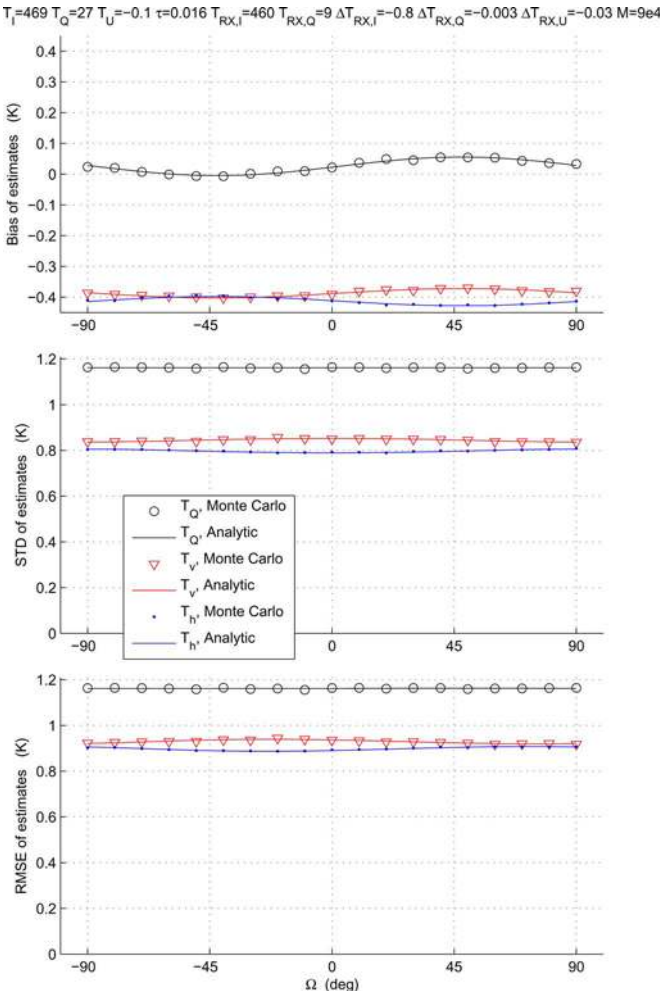

Fig. 3. Same as Fig. 1 except for the Hydros soil moisture sensing mission (different choices of $T_{\mathrm{RX},Q}$, $\Delta T_{\mathrm{RX},I}$, $\Delta T_{\mathrm{RX},Q}$, and $\Delta T_{\mathrm{RX},U}$ were also used in order to demonstrate the variety of possible behavior in the error).

numerical results and found patterns, then hypothesized the following formula for $\mathrm{Cov}(\hat{T}_{Ia},\hat{T}_Q)$ from those patterns:

$$\mathrm{Cov}(\hat{T}_{Ia},\hat{T}_Q) = \frac{2T_{\mathrm{sys},I}}{N}\sqrt{T_{\mathrm{sys},Q}^2+T_{\mathrm{sys},U}^2}. \tag{31}$$

Using (31) in (29) and (30)

$$\mathrm{Var}(\hat{T}_v) \approx \frac{2T_{\mathrm{sys},I}^2+4T_{\mathrm{sys},I}\sqrt{T_{\mathrm{sys},Q}^2+T_{\mathrm{sys},U}^2}+T_{\mathrm{sys},Q}^2+T_{\mathrm{sys},U}^2}{4N} \tag{32}$$

$$\mathrm{Var}(\hat{T}_h) \approx \frac{2T_{\mathrm{sys},I}^2-4T_{\mathrm{sys},I}\sqrt{T_{\mathrm{sys},Q}^2+T_{\mathrm{sys},U}^2}+T_{\mathrm{sys},Q}^2+T_{\mathrm{sys},U}^2}{4N}. \tag{33}$$

These, together with (27) and (28), give

$$\begin{aligned}&\text{Mean-square error of } \hat{T}_v \\ &\approx \frac{1}{4}\left[\sqrt{\sigma^2+m^2}-T_Q+\Delta T_{\mathrm{RX},I}\right]^2 \\ &\quad+\frac{2T_{\mathrm{sys},I}^2+4T_{\mathrm{sys},I}\sqrt{T_{\mathrm{sys},Q}^2+T_{\mathrm{sys},U}^2}+T_{\mathrm{sys},Q}^2+T_{\mathrm{sys},U}^2}{4N}\end{aligned} \tag{34}$$

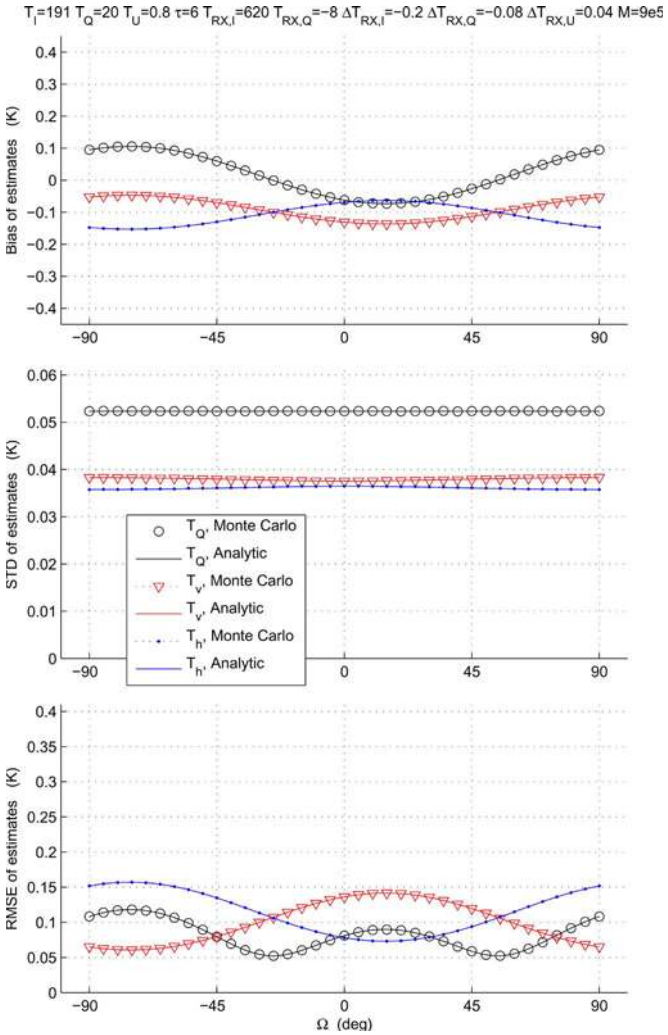

Fig. 4. Same as Fig. 1 except with the Monte Carlo results generated using the Gaussian approximation, thus allowing much larger M (different choices of $T_{\mathrm{RX},Q}$, $\Delta T_{\mathrm{RX},I}$, $\Delta T_{\mathrm{RX},Q}$, and $\Delta T_{\mathrm{RX},U}$ were also used in order to demonstrate the variety of possible behavior in the error).

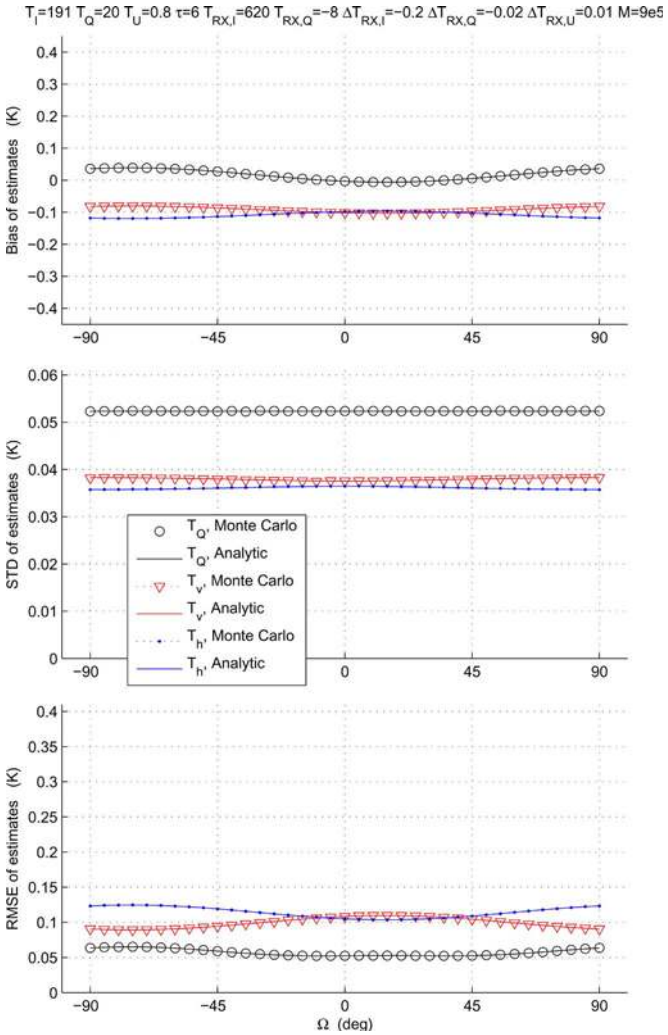

Fig. 5. Same as Fig. 4 except that we have chosen $\Delta T_{\mathrm{RX},Q}$ and $\Delta T_{\mathrm{RX},U}$ to be small compared to σ, which is the result anticipated from careful postlaunch calibration. As a consequence, the dependence on Ω is weak in this figure.

$$\text{Mean-square error of } \hat{T}_h \approx \frac{1}{4}\left[\sqrt{\sigma^2+m^2}-T_Q-\Delta T_{\mathrm{RX},I}\right]^2 + \frac{2T_{\mathrm{sys},I}^2-4T_{\mathrm{sys},I}\sqrt{T_{\mathrm{sys},Q}^2+T_{\mathrm{sys},U}^2}+T_{\mathrm{sys},Q}^2+T_{\mathrm{sys},U}^2}{4N}. \tag{35}$$

The RMSEs of the estimated T_v and T_h are the positive square roots of these equations. They do not appear to simplify further, although the variances can be approximated as $\sigma^2/2$.

B. Plots

In Figs. 1–4, we illustrate the (top) bias, (middle) STD, and (bottom) RMSE for the estimated T_Q, T_v, and T_h, as functions of Ω. The analytic results [given using (24)–(28) and (32)–(35)] are plotted as solid lines. The Monte Carlo results are plotted as symbols.

Figs. 1 and 2 were computed using T_I, T_Q [9], $T_{\mathrm{RX},I}$, and τ values that are typical of the innermost and outermost of the three Aquarius beams, respectively, while Fig. 3 uses values that are typical of the Hydros radiometer. The particular values of T_U, $T_{\mathrm{RX},Q}$, $\Delta T_{\mathrm{RX},I}$, and $\Delta T_{\mathrm{RX},Q}$ were chosen arbitrarily within their expected ranges. All values are given at the top of each figure. The Monte Carlo results were generated as previously described (Section IV-C2).

The discrepancies between the analytic and the Monte Carlo results decrease as M increases. But, it is difficult to increase M: generating a plot such as Fig. 1 currently requires days of computer time. Another option is to generate the Monte Carlo samples using the Gaussian approximation (see Section C in the Appendix). That is, rather than generating samples of the electric field, we generate samples of $\hat{T}_{Ia}$, $\hat{T}_{Qa}$, and $\hat{T}_{Ua}$ themselves as Gaussian random variables, with the means, variances, and covariances summarized in Section II. This method, although not quite as exact, is many orders of magnitude faster, allowing much larger M and more data points. Examples of the results obtained thereby are shown in Figs. 4 and 5.

VI. Insights From the Equations

With the forward model we have developed, there are five sources of error to be considered in PRC: T_U, $\Delta T_{\mathrm{RX},I}$,

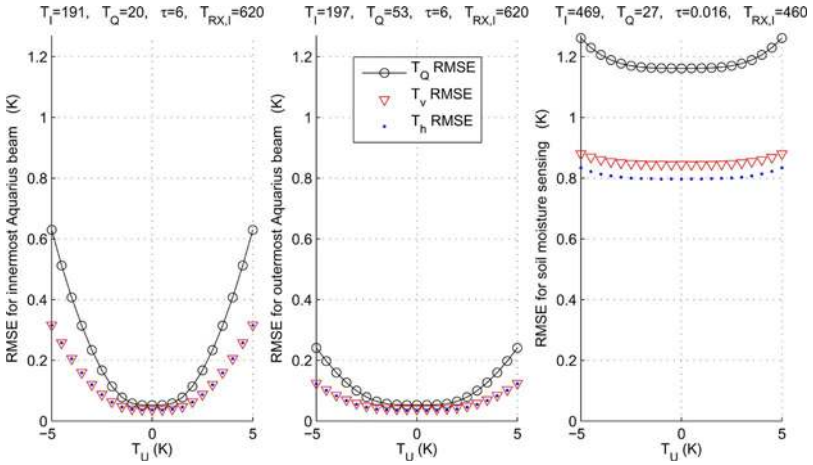

Fig. 6. RMSE (from the analytically derived formulas) of $\hat{T}_Q$, $\hat{T}_v$, and $\hat{T}_h$ as functions of T_U, with $\Delta T_{\mathrm{RX},I}$, $\Delta T_{\mathrm{RX},Q}$, and $\Delta T_{\mathrm{RX},U}$ set to zero. T_I, T_Q, τ, and $T_{\mathrm{RX},I}$ are typical of (left) the Aquarius $\theta = 28.7^\circ$ beam, (center) the Aquarius $\theta = 45.6^\circ$ beam, and (right) the Hydros soil moisture sensing mission.

$\Delta T_{\mathrm{RX},Q}$, $\Delta T_{\mathrm{RX},U}$, and $\mathrm{NE}\Delta T$ (manifested as σ). In this section, we study some effects of these error sources, using the equations derived previously. We note that after PRC, Ω can be viewed as merely a modulator of the error sources $\Delta T_{\mathrm{RX},Q}$ and $\Delta T_{\mathrm{RX},U}$ rather than as an error source in itself.

A. Insignificance of T_U

Examining (17), we see that the first term is desired while the rest are sources of bias. However, T_Q is more than an order of magnitude larger than the other components of (17); therefore, we can neglect terms without T_Q, resulting in

$$m^2 \approx T_Q^2 + 2T_Q(\Delta T_{\mathrm{RX},Q}\cos 2\Omega - \Delta T_{\mathrm{RX},U}\sin 2\Omega). \quad (36)$$

This eliminates T_U from the equations, which suggests that natural T_U is not a significant error source in PRC, at least at L-band.

We can numerically examine the significance of T_U as follows. We set the unknown error sources ($\Delta T_{\mathrm{RX},I}$, $\Delta T_{\mathrm{RX},Q}$, and $\Delta T_{\mathrm{RX},U}$) to zero but retain σ since it is known. Then, we plot RMSE as a function of natural T_U. The results are shown in Fig. 6 for the typical parameters of Aquarius beams. The RMSE at $T_U = 0$ is due to $\mathrm{NE}\Delta T$ through σ. We can discern that the error caused by natural T_U is negligible compared to $\mathrm{NE}\Delta T$ when $|T_U| < 1.5$ K.

Natural T_U is reported to have a maximum magnitude of about 1.5 K over the oceans at intermediate and high wind speeds, 10.7 GHz, and an incidence angle of 50° [17]. Extensive measurements at L-band have not been made, but one group reports amplitudes of less than 1 K over wind-driven ocean [18]. These measurements, combined with Fig. 6, suggest that natural T_U is not a significant error source for the Aquarius mission. This further suggests that the error allocation for "other (wind)" in the Aquarius error budget [6, p. 8] can be significantly reduced.

At the right of Fig. 6, we plot the results for typical parameters of a soil moisture sensing mission such as the canceled Hydros mission. The short integration time of this conical scanning radiometer results in $\mathrm{NE}\Delta T$ being so large that the effects of natural T_U are negligible for $|T_U| < 5$ K.

B. Optimal Ω Value

Examining (17) shows that near $\Omega = 0^\circ$, the effect of $\Delta T_{\mathrm{RX},Q}$ is amplified compared to the effect of $\Delta T_{\mathrm{RX},U}$, because of T_Q being so much larger than T_U. Similarly, the effect of $\Delta T_{\mathrm{RX},U}$ is amplified near $\Omega = 45^\circ$. Consequently, if $|\Delta T_{\mathrm{RX},Q}|$ is significantly larger than $|\Delta T_{\mathrm{RX},U}|$, then the RMSE of $\hat{T}_Q$ is minimum near $\Omega = 45^\circ$. Likewise, if $|\Delta T_{\mathrm{RX},Q}|$ is significantly smaller than $|\Delta T_{\mathrm{RX},U}|$, then the RMSE of $\hat{T}_Q$ is minimum near $\Omega = 0^\circ$ (see Figs. 1–4 for examples).

If $\Delta T_{\mathrm{RX},Q}$ and $\Delta T_{\mathrm{RX},U}$ have the same magnitude and sign, then RMSE is minimum near $\Omega = 22.5^\circ$. If they have the same magnitude but opposite sign, then RMSE is minimum near $\Omega = -22.5^\circ$. But, in all these cases, if the magnitude of both is less than $\sigma/2$, then RMSE is approximately constant with respect to Ω (and is $\approx\sigma$ for $\hat{T}_Q$), as shown in Fig. 5.

Because $\Delta T_{\mathrm{RX},Q}$ and $\Delta T_{\mathrm{RX},U}$ are unknown (at least until instrument fabrication and initial calibration), there is no basis for claiming *a priori* that RMSE is better at any one value of Ω than at any other value. This should correct the notion that it is best to sense the land or ocean at dawn because of low free electron content in the atmosphere (and, hence, small Ω), which is an assumption used in the design of the Hydros mission. We note that there may be other good reasons for sensing at dawn, such as the better known temperature profile of the atmosphere and planetary surface.

C. Negligible Error Contribution of PRC

If $\Delta T_{\mathrm{RX},I}$, $\Delta T_{\mathrm{RX},Q}$, and $\Delta T_{\mathrm{RX},U}$ are reduced to insignificance through postlaunch calibration, then the overall RMSE reduces to the $\mathrm{NE}\Delta T$ that exists regardless of polarization rotation. To see this analytically, let $\Delta T_{\mathrm{RX},I} = \Delta T_{\mathrm{RX},Q} = \Delta T_{\mathrm{RX},U} = 0$ and also let $T_U = 0$ since we know that its effect

is not large. Then, m^2 reduces to T_Q^2, and using a binomial expansion of (24)

$$\text{Bias}(\hat{T}_Q) \approx \sqrt{\sigma^2 + T_Q^2} - T_Q \approx \frac{\sigma^2}{2T_Q} \tag{37}$$

$$\Rightarrow \text{RMSE of } \hat{T}_Q \approx \sqrt{\sigma^2 + \frac{\sigma^4}{4T_Q^2}} \approx \sigma. \tag{38}$$

The validity of these approximations is easily confirmed by numerical examples using Aquarius and Hydros parameters.

Similar analysis shows that the RMSE of $\hat{T}_v$ and $\hat{T}_h$ reduces to $\sigma/2$. Hence, error allocation for ionospheric effects can be greatly reduced [6].

VII. Conclusion

We have extended the forward model of polarization rotation to include the random nature of radiation, radiometer channel noises, and (to first order) calibration. In particular, we have derived the means, variances, and covariances of the first three Stokes parameters T_I, T_Q, and T_U (or their modified counterparts, T_v, T_h, and T_U) as measured by radiometers in which T_U is measured as the correlation of T_v and T_h.

There are several known limitations to this forward model. First, it ignores the antenna sidelobe contributions to the apparent brightness temperature, which undergo a different amount of polarization rotation than the main beam contribution. Second, it ignores the mixing of the scene Stokes parameters by the antenna (i.e., the antenna cross-pol patterns). Third, it ignores the uncertainties in channel gains which remain after the calibration process. In this paper, we ignored these effects for tractability and because their effects are projected to be smaller than those effects which we have included.

Using the forward model just described, we have analyzed the errors in using polarimetric measurements to correct for polarization rotation as proposed in [1]. We have derived closed-form equations for the bias, STD, and RMSE of the estimated T_Q [see (24)–(26)] and similar expressions for T_v and T_h. These equations match the numerical results obtained by Monte Carlo simulation of our original electric-field model. These equations are the key results of this paper since they allow more accurate error analysis and error budgeting than has been possible previously.

This analysis indicates several things about the five sources of error. First, the natural third Stokes parameter (of the magnitude expected at L-band for most natural Earth scenes) is an insignificant source of error compared to $\text{NE}\Delta T$ (for $\tau \leq 6$ s over ocean).

Second, the dependence of RMSE on rotation angle is determined by residual errors from the calibration process $\Delta T_{\text{RX},Q}$ and $\Delta T_{\text{RX},U}$. Since these residuals are unknown (by definition), we cannot predict the dependence of RMSE on rotation angle (such as whether or not $\Omega = 0^\circ$ is the optimum angle). But, if the postlaunch calibration reduces $\Delta T_{\text{RX},Q}$ and $\Delta T_{\text{RX},U}$ to the level of $\text{NE}\Delta T$ or less, then the dependence of RMSE on Ω is weak.

Third, if $\Delta T_{\text{RX},I}$, $\Delta T_{\text{RX},Q}$, and $\Delta T_{\text{RX},U}$ are reduced to insignificance through postlaunch calibration, then the overall RMSE reduces to the $\text{NE}\Delta T$ that exists regardless of polarization rotation. In other words, Yueh's method reduces the error incurred by the polarization rotation to negligibility.

Appendix I

In this Appendix, we derive (1)–(3). These equations comprise the forward model of polarization rotation which is used in this paper.

A. Electric-Field Model

Our most basic foundation is a model of the electric fields

$$\begin{bmatrix} x(t) \\ y(t) \end{bmatrix} = \begin{bmatrix} \cos\Omega & \sin\Omega \\ -\sin\Omega & \cos\Omega \end{bmatrix} \begin{bmatrix} E_v(t) \\ E_h(t) \end{bmatrix} + \begin{bmatrix} a(t) \\ b(t) \end{bmatrix}. \tag{39}$$

$E_v(t)$ and $E_h(t)$ are the components of the total electric field emitted by the scene in the vertical and horizontal directions, respectively (hereafter, our notation suppresses the time dependence t of all quantities). Because the number of independent emitters in the scene is large in spaceborne radiometry, E_v and E_h are normally distributed, by the central limit theorem, with zero means [19, pp. 477–478]. We assume that they are real because we are concerned only with the first three Stokes parameter in this paper.

E_v and E_h are rotated through an angle Ω, modeling polarization rotation. We consider Ω to be constant over the period of one radiometer measurement. Receiver noise is then added, which is represented by the electric field amplitudes a and b. Like E_v and E_h, we assume that a and b are normally distributed, zero mean, and normal random variables. We also assume that they are independent of one another and of E_v and E_h. They represent self-emission by the antenna and radiometer. This model neglects the sidelobe contributions (as they may undergo different amounts of rotation than the main beam radiation) and cross coupling of the polarization components that is caused by the antenna and radiometer nonidealities (cross-pol patterns).

The quantities that are most commonly reported in radiometry are the first three modified Stokes parameters, as brightness temperatures

$$\begin{bmatrix} T_v \\ T_h \\ T_U \end{bmatrix} \equiv \begin{bmatrix} \langle E_v^2 \rangle \\ \langle E_h^2 \rangle \\ 2\langle E_v E_h \rangle \end{bmatrix} \tag{40}$$

to which we add, for this document

$$\begin{bmatrix} T_{\text{RX},v} \\ T_{\text{RX},h} \end{bmatrix} \equiv \begin{bmatrix} \langle a^2 \rangle \\ \langle b^2 \rangle \end{bmatrix}. \tag{41}$$

In these and subsequent definitions, we ignore a proportionality constant which converts the product of two electric fields to a brightness temperature. This conversion also assumes a narrowband radiometer, so that the frequency spectrums of $E_v(t)$, $E_h(t)$, $a(t)$, and $b(t)$ are flat (see [12, p. 193]).

A quantity of high interest to users of radiometry data is the second Stokes parameter $T_Q \equiv T_v - T_h \equiv \langle E_v^2 \rangle - \langle E_h^2 \rangle$, where $\langle \cdot \rangle$ denotes the expected value (ensemble average). In addition to the definition in (40), T_U can be equivalently defined in a manner analogous to the definition of T_Q. This definition is $T_U \equiv T_{+45} - T_{-45}$, where T_{+45} is the brightness temperature of the component of the incident radiation that is linearly polarized at 45° with respect to the E_v and E_h axes.

Our model assumes a radiometer architecture in which the signals at $+45^\circ$ and -45° linear polarization (in the radiometer polarization basis) are synthesized from x and y after enough amplification of x and y (by amplifiers) that the receiver noise added after this synthesis is negligible. Radiometers which create the signals at $+45^\circ$ and -45° earlier (such as from direct measurement of T_{+45} and T_{-45}) require that additional noise terms should be added to the additional channels. This would add many terms to the final forward model and the error formulas.

B. Description of Parameters

In this document, we could express our results in terms of T_v, T_h, $T_{\mathrm{RX},v}$, and $T_{\mathrm{RX},h}$. It is more concise, however, to use the related quantities $T_I \equiv T_v + T_h$, $T_Q \equiv T_v - T_h$, $T_{\mathrm{RX},I} \equiv T_{\mathrm{RX},v} + T_{\mathrm{RX},h}$, and $T_{\mathrm{RX},Q} \equiv T_{\mathrm{RX},v} - T_{\mathrm{RX},h}$. Note that T_I, T_Q, and T_U comprise the first three Stokes parameters [7] as brightness temperatures. We also note that in the final expressions for bias and variance (and, hence, RMSE), T_I and $T_{\mathrm{RX},I}$ always appear added together, never separately. Therefore, we reduce our parameter set by using $T_{\mathrm{sys},I} \equiv T_I + T_{\mathrm{RX},I}$.

Besides T_I, T_Q, T_U, $T_{\mathrm{RX},I}$, and $T_{\mathrm{RX},Q}$, other parameters are Ω, N, $\Delta T_{\mathrm{RX},I}$, $\Delta T_{\mathrm{RX},Q}$, and $\Delta T_{\mathrm{RX},U}$ (N is defined early in Appendix I-C; $\Delta T_{\mathrm{RX},I}$, $\Delta T_{\mathrm{RX},Q}$, and $\Delta T_{\mathrm{RX},U}$ are defined in Appendix I-E). This collection of ten parameters can be used to completely describe the forward problem, and we, therefore, refer to them as the "original parameters." Other quantities are defined for convenience but can be expressed in terms of these original ten.

The symbols x and y represent the electric fields to be detected by the radiometer. By the construction of (39), they are also zero-mean normal random variables. We denote their expected squared values, as brightness temperatures, with

$$\begin{bmatrix} T_{\mathrm{sys},v} \\ T_{\mathrm{sys},h} \\ T_{\mathrm{sys},U} \end{bmatrix} \equiv \begin{bmatrix} \langle x^2 \rangle \\ \langle y^2 \rangle \\ 2\langle xy \rangle \end{bmatrix}. \tag{42}$$

Using (40), (41), and the facts that a and b are independent of all other quantities and are zero mean, we find

$$\begin{aligned} T_{\mathrm{sys},v} &= \left\langle (E_v \cos\Omega + E_h \sin\Omega + a)^2 \right\rangle \\ &= T_v \cos^2\Omega + T_h \sin^2\Omega + \frac{T_U}{2}\sin 2\Omega + T_{\mathrm{RX},v}. \end{aligned} \tag{43}$$

By a similar process

$$T_{\mathrm{sys},h} = T_h \cos^2\Omega + T_v \sin^2\Omega - \frac{T_U}{2}\sin 2\Omega + T_{\mathrm{RX},h} \tag{44}$$

$$T_{\mathrm{sys},U} = -T_Q \sin 2\Omega + T_U \cos 2\Omega. \tag{45}$$

C. Measured Temperatures, $\hat{T}_{\mathrm{sys},v}$, $\hat{T}_{\mathrm{sys},h}$ and $\hat{T}_{\mathrm{sys},U}$

A conventional two-channel radiometer measures $T_{\mathrm{sys},v}$ and $T_{\mathrm{sys},h}$ by a time average

$$\hat{T}_{\mathrm{sys},v} \equiv \frac{1}{\tau}\int_0^\tau x^2 dt, \quad \hat{T}_{\mathrm{sys},h} \equiv \frac{1}{\tau}\int_0^\tau y^2 dt. \tag{46}$$

We use hats to denote measured or estimated quantities, which are random variables, as opposed to the unhatted quantities which represent the desired true quantities, such as the ensemble average of a random variable.

A three-channel polarimetric radiometer also measures

$$\hat{T}_{\mathrm{sys},U} \equiv \frac{2}{\tau}\int_0^\tau xy\, dt. \tag{47}$$

As shown in [19, pp. 487–488], $\hat{T}_{\mathrm{sys},v}$, $\hat{T}_{\mathrm{sys},h}$, and $\hat{T}_{\mathrm{sys},U}$ can be rewritten as sums of independent samples

$$\begin{aligned} \hat{T}_{\mathrm{sys},v} &= \frac{1}{N}\sum_{i=1}^N x_i^2 \\ \hat{T}_{\mathrm{sys},h} &= \frac{1}{N}\sum_{i=1}^N y_i^2 \\ \hat{T}_{\mathrm{sys},U} &= \frac{2}{N}\sum_{i=1}^N x_i y_i \end{aligned} \tag{48}$$

where $N = 2B\tau$, B is the sensor bandwidth, and τ is the integration time.

We next proceed to find the distributions of $\hat{T}_{\mathrm{sys},v}$, $\hat{T}_{\mathrm{sys},h}$, and $\hat{T}_{\mathrm{sys},U}$. For large N (for Aquarius, $N \approx 5e8$), $\hat{T}_{\mathrm{sys},v}$ is so nearly Gaussian, by the central limit theorem, that we assume that it is Gaussian. Similar results apply for $\hat{T}_{\mathrm{sys},h}$ and $\hat{T}_{\mathrm{sys},U}$. Therefore, they can be very well characterized by only their means, variances, and covariances, which we derive next.

1) Means of $\hat{T}_{\mathrm{sys},v}$, $\hat{T}_{\mathrm{sys},h}$, and $\hat{T}_{\mathrm{sys},U}$: The ensemble average (expected value) of $\hat{T}_{\mathrm{sys},v}$ is

$$\langle \hat{T}_{\mathrm{sys},v} \rangle = \left\langle \frac{1}{N}\sum_{i=1}^N x_i^2 \right\rangle = \frac{1}{N}\sum_{i=1}^N \langle x_i^2 \rangle = T_{\mathrm{sys},v}. \tag{49}$$

Similarly, $\langle \hat{T}_{\mathrm{sys},h} \rangle = T_{\mathrm{sys},h}$ and $\langle \hat{T}_{\mathrm{sys},U} \rangle = T_{\mathrm{sys},U}$.

2) $\mathrm{Var}(\hat{T}_{\mathrm{sys},v})$ *and* $\mathrm{Var}(\hat{T}_{\mathrm{sys},h})$*:*

$$\begin{aligned} \mathrm{Var}(\hat{T}_{\mathrm{sys},v}) &= \left\langle \left(\frac{1}{N}\sum_{i=1}^N x_i^2\right)\left(\frac{1}{N}\sum_{j=1}^N x_j^2\right) \right\rangle - T_{\mathrm{sys},v}^2 \\ &= \left\langle \frac{1}{N^2}\sum_{i=1}^N\sum_{j=1}^N x_i^2 x_j^2 \right\rangle - T_{\mathrm{sys},v}^2 \end{aligned} \tag{50}$$

which we separate into terms for which $i \neq j$ and for which $i = j$

$$= \frac{1}{N^2}\sum_{i=1}^{N}\sum_{j=1(\neq i)}^{N}\langle x_i^2 x_j^2\rangle + \frac{1}{N^2}\sum_{i=1}^{N}\langle x_i^4\rangle - T_{\mathrm{sys},v}^2. \quad (51)$$

Using the independence of samples i and j and the known fourth moment of zero-mean normal random variables

$$= \frac{1}{N^2}\sum_{i=1}^{N}\langle x_i^2\rangle\sum_{j=1(\neq i)}^{N}\langle x_j^2\rangle + \frac{1}{N^2}\sum_{i=1}^{N}3\langle x_i^2\rangle^2 - T_{\mathrm{sys},v}^2. \quad (52)$$

Then, using (42)

$$\mathrm{Var}(\hat{T}_{\mathrm{sys},v}) = \frac{2}{N}T_{\mathrm{sys},v}^2. \quad (53)$$

By a similar process

$$\mathrm{Var}(\hat{T}_{\mathrm{sys},h}) = \frac{2}{N}T_{\mathrm{sys},h}^2. \quad (54)$$

3) $\mathrm{Var}(\hat{T}_{\mathrm{sys},U})$*:* By a process similar to (50)–(53)

$$\mathrm{Var}(\hat{T}_{\mathrm{sys},U}) = \frac{-T_{\mathrm{sys},U}^2}{N} + \frac{4}{N}\langle x^2y^2\rangle. \quad (55)$$

Consider $\langle x^2y^2\rangle$ alone. Using the definitions of x and y in (39), it can be expanded to several dozen terms. The independence of a and b from E_v and E_h means that many terms can be factored as $\langle a\rangle$, $\langle b^2\rangle$, and so on. Then, using (40), (41), the fact that a and b are zero mean, and the known fourth moment of zero-mean normal random variables, many terms drop out or simplify, leaving

$$\begin{aligned}\langle x^2y^2\rangle = {} & \frac{1}{2}\left\langle E_vE_h^3 - E_v^3E_h\right\rangle\sin 4\Omega + \frac{1}{2}T_IT_{\mathrm{RX},I} \\ & + \left(\frac{3}{4}\left\langle E_v^2E_h^2\right\rangle - \frac{3}{8}\left(T_v^2+T_h^2\right)\right)\cos 4\Omega \\ & - \frac{1}{2}T_{\mathrm{RX},Q}(T_U\sin 2\Omega + T_Q\cos 2\Omega) + \frac{3}{8}T_v^2 \\ & + \frac{1}{4}\left\langle E_v^2E_h^2\right\rangle + \frac{3}{8}T_h^2 + T_{\mathrm{RX},v}T_{\mathrm{RX},h}. \end{aligned} \quad (56)$$

E_v and E_h are marginally zero-mean Gaussians, with variances of T_v and T_h and a covariance of $T_U/2$. Assuming that they are jointly Gaussian, their joint pdf is completely specified. We can therefore determine $\langle E_v^3E_h\rangle$, $\langle E_vE_h^3\rangle$, and $\langle E_v^2E_h^2\rangle$ by direct integration

$$\begin{aligned}\left\langle E_v^3E_h\right\rangle = {} & \frac{1}{\pi\sqrt{4T_vT_h - T_U^2}} \\ & \cdot\int_{-\infty}^{\infty}\int_{-\infty}^{\infty}E_v^3E_h e^{\frac{-2T_hE_v^2+2T_UE_hE_v-2T_vE_h^2}{4T_vT_h-T_U^2}}dE_vdE_h. \end{aligned} \quad (57)$$

Using a table of integrals [20], the known second and fourth moments of zero-mean Gaussians, and much algebra, this reduces to

$$\left\langle E_v^3E_h\right\rangle = \frac{3}{2}T_UT_v. \quad (58)$$

By similar processes, we find

$$\begin{aligned}\left\langle E_vE_h^3\right\rangle &= \frac{3}{2}T_UT_h \\ \left\langle E_v^2E_h^2\right\rangle &= T_vT_h + \frac{1}{2}T_U^2. \end{aligned} \quad (59)$$

By using these results in (56) and then using (56) in (55), we obtain, after much algebraic manipulation

$$\mathrm{Var}(\hat{T}_{\mathrm{sys},U}) = \frac{1}{N}\left[T_{\mathrm{sys},I}^2 - T_{\mathrm{sys},Q}^2 + T_{\mathrm{sys},U}^2\right] \quad (60)$$

where $T_{\mathrm{sys},I} \equiv T_{\mathrm{sys},v} + T_{\mathrm{sys},h} = T_I + T_{\mathrm{RX},I}$ and $T_{\mathrm{sys},Q} \equiv T_{\mathrm{sys},v} - T_{\mathrm{sys},h}$.

4) Covariances of $\hat{T}_{\mathrm{sys},v}$*,* $\hat{T}_{\mathrm{sys},h}$*, and* $\hat{T}_{\mathrm{sys},U}$*:* We wish to determine the covariances that exist between $\hat{T}_{\mathrm{sys},v}$, $\hat{T}_{\mathrm{sys},h}$, and $\hat{T}_{\mathrm{sys},U}$. Similar to the derivation of (60), it can be shown that

$$\mathrm{Cov}(\hat{T}_{\mathrm{sys},v},\hat{T}_{\mathrm{sys},h}) = \frac{T_{\mathrm{sys},U}^2}{2N} \quad (61)$$

$$\mathrm{Cov}(\hat{T}_{\mathrm{sys},v},\hat{T}_{\mathrm{sys},U}) = \frac{2T_{\mathrm{sys},v}T_{\mathrm{sys},U}}{N} \quad (62)$$

$$\mathrm{Cov}(\hat{T}_{\mathrm{sys},h},\hat{T}_{\mathrm{sys},U}) = \frac{2T_{\mathrm{sys},h}T_{\mathrm{sys},U}}{N}. \quad (63)$$

D. Definition and Characterization of $\hat{T}_{\mathrm{sys},I}$ *and* $\hat{T}_{\mathrm{sys},Q}$

It is more convenient to work with the sum and difference of $\hat{T}_{\mathrm{sys},v}$ and $\hat{T}_{\mathrm{sys},h}$ than with these quantities themselves. Therefore, we define $\hat{T}_{\mathrm{sys},I} \equiv \hat{T}_{\mathrm{sys},v} + \hat{T}_{\mathrm{sys},h}$, and $\hat{T}_{\mathrm{sys},Q} \equiv \hat{T}_{\mathrm{sys},v} - \hat{T}_{\mathrm{sys},h}$. Using the formulas given previously, it is straightforward to show that

$$\langle\hat{T}_{\mathrm{sys},I}\rangle = T_I + T_{\mathrm{RX},I} = T_{\mathrm{sys},I} \quad (64)$$

$$\langle\hat{T}_{\mathrm{sys},Q}\rangle = T_Q\cos 2\Omega + T_U\sin 2\Omega + T_{\mathrm{RX},Q} = T_{\mathrm{sys},Q} \quad (65)$$

and that the variances and covariances of $\hat{T}_{\mathrm{sys},I}$, $\hat{T}_{\mathrm{sys},Q}$, and $\hat{T}_{\mathrm{sys},U}$ can be summarized with the symmetric covariance matrix given in (66), shown at the top of the next page.

E. Forward Model of Rotated and Calibrated Brightness Temperatures

As discussed at the beginning of Appendix I-C, the measured temperatures are normal random variables with the means and variances that were just found. It is convenient to break them up into the sum of their means and zero-mean normal random variables

$$\begin{bmatrix}\hat{T}_{\mathrm{sys},v}\\ \hat{T}_{\mathrm{sys},h}\\ \hat{T}_{\mathrm{sys},U}\end{bmatrix} \equiv \begin{bmatrix}T_{\mathrm{sys},v}+\Delta T_{\mathrm{sys},v}\\ T_{\mathrm{sys},h}+\Delta T_{\mathrm{sys},h}\\ T_{\mathrm{sys},U}+\Delta T_{\mathrm{sys},U}\end{bmatrix} \quad (67)$$

$$\begin{bmatrix} \mathrm{Var}(\hat{T}_{\mathrm{sys},I}) & \mathrm{Cov}(\hat{T}_{\mathrm{sys},I},\hat{T}_{\mathrm{sys},Q}) & \mathrm{Cov}(\hat{T}_{\mathrm{sys},I},\hat{T}_{\mathrm{sys},U}) \\ & \mathrm{Var}(\hat{T}_{\mathrm{sys},Q}) & \mathrm{Cov}(\hat{T}_{\mathrm{sys},Q},\hat{T}_{\mathrm{sys},U}) \\ & & \mathrm{Var}(\hat{T}_{\mathrm{sys},U}) \end{bmatrix}$$
$$= \frac{1}{N} \cdot \begin{bmatrix} T_{\mathrm{sys},I}^2 + T_{\mathrm{sys},Q}^2 + T_{\mathrm{sys},U}^2 & 2T_{\mathrm{sys},I}T_{\mathrm{sys},Q} & 2T_{\mathrm{sys},I}T_{\mathrm{sys},U} \\ & T_{\mathrm{sys},I}^2 + T_{\mathrm{sys},Q}^2 - T_{\mathrm{sys},U}^2 & 2T_{\mathrm{sys},Q}T_{\mathrm{sys},U} \\ & & T_{\mathrm{sys},I}^2 - T_{\mathrm{sys},Q}^2 + T_{\mathrm{sys},U}^2 \end{bmatrix} \quad (66)$$

and similarly for the quantities defined for convenience

$$\hat{T}_{\mathrm{sys},I} \equiv T_{\mathrm{sys},I} + \Delta T_{\mathrm{sys},I} \quad (68)$$

$$\hat{T}_{\mathrm{sys},Q} \equiv T_{\mathrm{sys},Q} + \Delta T_{\mathrm{sys},Q} \quad (69)$$

where $\Delta T_{\mathrm{sys},I} \equiv \Delta T_{\mathrm{sys},v} + \Delta T_{\mathrm{sys},h}$ and $\Delta T_{\mathrm{sys},Q} \equiv \Delta T_{\mathrm{sys},v} - \Delta T_{\mathrm{sys},h}$.

Expanding these out in terms of the original parameters, we have

$$\hat{T}_{\mathrm{sys},v} = T_v - T_Q \sin^2\Omega + \frac{T_U}{2}\sin 2\Omega + T_{\mathrm{RX},v} + \Delta T_{\mathrm{sys},v}$$

$$\hat{T}_{\mathrm{sys},h} = T_h + T_Q \sin^2\Omega - \frac{T_U}{2}\sin 2\Omega + T_{\mathrm{RX},h} + \Delta T_{\mathrm{sys},h}$$

$$\hat{T}_{\mathrm{sys},U} = -T_Q \sin 2\Omega + T_U \cos 2\Omega + \Delta T_{\mathrm{sys},U} \quad (70)$$

$$\hat{T}_{\mathrm{sys},I} = T_I + T_{\mathrm{RX},I} + \Delta T_{\mathrm{sys},I} \quad (71)$$

$$\hat{T}_{\mathrm{sys},Q} = T_Q \cos 2\Omega + T_U \sin 2\Omega + T_{\mathrm{RX},Q} + \Delta T_{\mathrm{sys},Q}. \quad (72)$$

Now, note that $T_{\mathrm{RX},v}$ and $T_{\mathrm{RX},h}$ (and, hence, also their sum and difference $T_{\mathrm{RX},I}$ and $T_{\mathrm{RX},Q}$) are operationally estimated and subtracted off as part of the radiometer data calibration. Imperfection in this correction leaves residuals which we call $\Delta T_{\mathrm{RX},v}$ and $\Delta T_{\mathrm{RX},h}$. It is convenient to also define $\Delta T_{\mathrm{RX},I} \equiv \Delta T_{\mathrm{RX},v} + \Delta T_{\mathrm{RX},h}$ and $\Delta T_{\mathrm{RX},Q} \equiv \Delta T_{\mathrm{RX},v} - \Delta T_{\mathrm{RX},h}$. With $T_{\mathrm{RX},v}$, $T_{\mathrm{RX},h}$, $T_{\mathrm{RX},I}$ and $T_{\mathrm{RX},Q}$ subtracted off and leaving only these residuals, we finally have a forward model for the outputs of the rotation, measurement, and calibration processes, which become the inputs to the PRC process of [1]. Using a notation similar to [1] for these inputs, where the subscript "a" can be interpreted as referring to temperatures "after" rotation, measurement, and calibration,

$$\hat{T}_{va} = T_v - T_Q \sin^2\Omega + \frac{T_U}{2}\sin 2\Omega + \Delta T_{\mathrm{RX},v} + \Delta T_{\mathrm{sys},v} \quad (73)$$

$$\hat{T}_{ha} = T_h + T_Q \sin^2\Omega - \frac{T_U}{2}\sin 2\Omega + \Delta T_{\mathrm{RX},h} + \Delta T_{\mathrm{sys},h} \quad (74)$$

$$\hat{T}'_{Ua} = -T_Q \sin 2\Omega + T_U \cos 2\Omega + \Delta T_{\mathrm{sys},U}. \quad (75)$$

As explained in Section II, the measurement and calibration process also add a residual bias $\Delta T_{\mathrm{RX},U}$ to this last equation, as included in (3).

Equations (73) and (74) are the generalizations of [1, eqs. (12) and (13)]. For convenience, we use the sum and difference of (73) and (74), as given in (1) and (2), respectively.

REFERENCES

[1] S. H. Yueh, "Estimates of Faraday rotation with passive microwave polarimetry for microwave remote sensing of Earth surfaces," *IEEE Trans. Geosci. Remote Sens.*, vol. 38, no. 5, pp. 2434–2438, Sep. 2000.

[2] D. M. Le Vine and S. Abraham, "The effect of the ionosphere on remote sensing of sea surface salinity from space: Absorption and emission at L-band," *IEEE Trans. Geosci. Remote Sens.*, vol. 40, no. 4, pp. 771–782, Apr. 2002.

[3] T. Meissner and F. J. Wentz, "Polarization rotation and the third Stokes parameter: The effects of spacecraft attitude and Faraday rotation," *IEEE Trans. Geosci. Remote Sens.*, vol. 44, no. 3, pp. 506–515, Mar. 2006.

[4] A. J. Gasiewski and D. B. Kunkee, "Calibration and applications of polarization-correlating radiometers," *IEEE Trans. Microw. Theory Tech.*, vol. 41, no. 5, pp. 767–773, May 1993.

[5] I. Corbella, F. Torres, A. Camps, A. Colliander, M. Martín-Neira, S. Ribó, K. Rautiainen, N. Duffo, and M. Vall-llossera, "MIRAS end-to-end calibration: Application to SMOS L1 processor," *IEEE Trans. Geosci. Remote Sens.*, vol. 43, no. 5, pp. 1126–1134, May 2005.

[6] Aquarius Team, *Aquarius Selected Instrument Concept*, Greenbelt, MD: Goddard Space Flight Center. [Online]. Available: http://aquarius.gsfc.nasa.gov/pdf/instrument.pdf

[7] S. Chandrasekhar, *Radiative Transfer*, ser. The International Series of Monographs on Physics. Oxford, U.K.: Clarendon, 1950.

[8] S. Ribó and M. Martín-Neira, "Faraday rotation correction in the polarimetric mode of MIRAS," *IEEE Trans. Geosci. Remote Sens.*, vol. 42, no. 7, pp. 1405–1410, Jul. 2004.

[9] Y. Kerr, P. Waldteufel, and F. Cabot. (2004, Sep.). *SMOS geolocation using natural targets*. [Online]. Available: http://www.cesbio.ups-tlse.fr/data_all/SMOS-doc/geolocation.pdf

[10] D. Entekhabi, E. G. Njoku, P. Houser, M. Spencer, T. Doiron, Y. Jim, J. Smith, R. Girard, S. Belair, W. Crow, T. J. Jackson, Y. H. Kerr, J. S. Kimball, R. Koster, K. C. McDonald, P. E. O'Neill, T. Pultz, S. W. Running, J. Shi, E. Wood, and J. van Zyl, "The Hydrosphere State (Hydros) satellite mission: An Earth system pathfinder for global mapping of soil moisture and land freeze/thaw," *IEEE Trans. Geosci. Remote Sens.*, vol. 42, no. 10, pp. 2184–2195, Oct. 2004.

[11] J. R. Piepmeier, "Calibration of passive microwave polarimeters that use hybrid coupler-based correlators," *IEEE Trans. Geosci. Remote Sens.*, vol. 42, no. 2, pp. 391–400, Feb. 2004.

[12] F. T. Ulaby, R. K. Moore, and A. K. Fung, *Microwave Remote Sensing: Active and Passive*, vol. 1. Norwood, MA: Artech House, 1981.

[13] H. Weil, "The distribution of radial error," *Ann. Math. Stat.*, vol. 25, no. 1, pp. 168–170, Mar. 1954.

[14] A. Papoulis, *Probability, Random Variables, and Stochastic Processes*, 3rd ed. New York: McGraw-Hill, 1991. exercise 6–16.

[15] K. S. Miller, *Multidimensional Gaussian Distributions*, ser. SIAM Series in Applied Mathematics. New York: Wiley, 1964.

[16] S. O. Rice, "Mathematical analysis of random noise—Conclusion," *Bell Syst. Tech. J.*, vol. 24, no. 1, pp. 46–156, 1945.

[17] S. H. Yueh, W. J. Wilson, S. J. Dinardo, and S. V. Hsiao, "Polarimetric microwave wind radiometer model function and retrieval testing for WindSat," *IEEE Trans. Geosci. Remote Sens.*, vol. 44, no. 3, pp. 584–596, Mar. 2006.

[18] S. S. Sobjaerg, J. Rotboll, and N. Skou, "Measurement of wind signatures on the sea surface using an L-band polarimetric radiometer," in *Proc. IEEE Int. Geosci. and Remote Sens. Symp.*, 2002, vol. 3, pp. 1364–1366.

[19] F. T. Ulaby, R. K. Moore, and A. K. Fung, *Microwave Remote Sensing: Active and Passive*, vol. 2. Norwood, MA: Artech House, 1986, ch. 7.
[20] I. S. Gradshteyn and I. M. Ryzhik, *Tables of Integrals, Series, and Products*, 4th ed. New York: Academic, 1965. Sec. 3.462.

Derek Hudson received the B.S. and M.S. degrees in electrical engineering from Brigham Young University (BYU), Provo, UT, in 2003. He is currently working toward the Ph.D. degree in electrical engineering at BYU.

He has been with the Microwave Earth Remote Sensing research group at BYU since 1999. His research experience is in the application of inverse problem theory and in radar hardware design.

Jeffrey R. Piepmeier (S'89–M'99) received the B.S. degree in engineering from LeTourneau University, Longview, TX, in 1993, the M.S. and Ph.D. degrees in electrical engineering from the Georgia Institute of Technology (Georgia Tech.), Atlanta, in 1994 and 1999, respectively.

From 1993 to 1994, he was a Schakleford Fellow with the Georgia Tech Research Institute. Since 1999, he has been with the Microwave Instrument Technology Branch, NASA Goddard Space Flight Center, Greenbelt, MD. Currently, he is the Prelaunch Calibration Lead Engineer for the Aquarius/SAC-D mission. His technical interests include passive remote sensing and technology development for microwave remote sensing.

Dr. Piepmeier was the third place winner in the 1998 IGARSS student Prize Paper competition. He was the recipient of an Excellence in Federal Career Gold Award (Rookie-of-theYear) in 2000 and was a 2002 NASA Earth Science New Investigator. In 2000, he served as the Conference Chair of the First Microwave Radiometer Calibration Workshop (MicroCal2000). He was the Cochairman/Chairman of the Instrumentation and Future Technologies Technical Committee of the IEEE Geoscience and Remote Sensing Society from 2000 to 2006. He is currently the Cochairman of the NAS Committee on Radio Frequencies. He is a member of Union Radio-Scientifique Internationale (Commission F) and the American Geophysical Union.

David G. Long (S'80–SM'98) received the Ph.D. degree in electrical engineering from University of Southern California, Los Angeles, CA, in 1989.

From 1983 to 1990, he worked for NASA's Jet Propulsion Laboratory (JPL), Pasadena, CA, where he developed the advanced radar remote sensing systems. While at JPL, he was the Project Engineer on the NASA Scatterometer (NSCAT) project which flew from 1996 to 1997. He also managed the SCANSCAT project, which is the precursor to SeaWinds which was launched in 1999 and 2002. He is currently a Professor in the Department of Electrical and Computer Engineering, Brigham Young University (BYU), Provo, UT, where he teaches upper division and graduate courses in communications, microwave remote sensing, radar, and signal processing and is the Director of the BYU Center for Remote Sensing. He is the Principal Investigator on several NASA-sponsored research projects in remote sensing. He has numerous publications in signal processing and radar scatterometry. His research interests include microwave remote sensing, radar theory, space-based sensing, estimation theory, signal processing, and mesoscale atmospheric dynamics. He has over 275 publications.

Dr. Long has received the NASA Certificate of Recognition several times. He is an Associate Editor for IEEE GEOSCIENCE AND REMOTE SENSING LETTERS.